Earthquakes triggered by the subsurface undrained response to reservoir-impoundment at Irapé, Brazil

Haris Raza[1,2,3]*, George Sand França[1,2], Eveline Sayão[1], Victor Vilarrasa[3]

[1]Seismological Observatory, Graduate Program in Geology, Institute of Geosciences, University of Brasília, Campus Darcy Ribeiro, 70297-400 Brasília, Brazil

[2]Institute of Astronomy, Geophysics and Atmospheric Sciences, University of São Paulo, 05508-090, São Paulo, Brazil

[3]Global Change Research Group (GCRG), IMEDEA, CSIC-UIB, 07190 Esporles, Spain

*Correspondence to: Haris Raza (harisraza90@yahoo.com), Victor Vilarrasa (victor.vilarrasa@csic.es)

Abstract

The necessity to reduce carbon emissions to mitigate climate change is accelerating the transition from fossil fuels to renewable energy sources. Specifically, hydropower ~~in particular~~ has emerged as a prominent and safe renewable energy source, but entails reservoir-triggered seismicity (RTS). This phenomenon causes significant challenges for safe reservoir management. Irapé, in Brazil, is a prominent RTS site where seismicity surged after reservoir filling, with a maximum event of magnitude 3.0 in May 2006, just six months after the start of reservoir impoundment. Despite more than a decade has passed since the seismicity occurred, the factors governing these earthquakes and their connection to subsurface rock properties remain poorly understood. Here, we attempt to understand the potential causes of RTS at Irapé dam, which is the highest dam in Brazil with 208 m, and the second highest in South America. Permeability and porosity measurements of cylindrical cores from hard and intact rock samples which have been extracted near the RTS zone, by pitting 10 cm from the surface reveal a low-permeability rock. Porosity values range from 6.3 to 14.7%. Only three out of the eleven tested samples present permeability ~~higher than~~ above the lowest measurable value of the apparatus (0.002 mD), with the highest permeability being 0.0098 mD. The undrained response of the low-permeability rock placed below the reservoir results in an instantaneous increase in pore pressure and poroelastic stress changes due to elastic compression, which brings potential faults located below the reservoir closer to failure conditions. According to our analytical calculations, the vertical loading caused by the increase in 136 m of the reservoir-water level caused lead to a ~~0.54~~ 0.61 MPa pore pressure buildup in response to compression at the depth of the Magnitude 3.0 earthquake, i.e., 3.88 km, resulting in an increase

of 0.82 0.75 MPa in the vertical effective stress and a decrease of 0.34 0.48 MPa in the horizontal effective stress. These changes resulted in an increase in the deviatoric stress that led to fault destabilization, causing the RTS. The laboratory measurements and analytical calculations corroborate the hypothesis that the initial seismic activity was induced by the undrained subsurface response to the reservoir loading at Irapé.

Keywords: Brazil, Reservoir-triggered seismicity, Permeability, Porosity, Fault, Reservoir-management

1.Introduction

Reservoir impoundment, deep underground mining, and fluid injection into and withdrawal from the subsurface are some of the well-known causes of induced/triggered seismicity which have become a global issue in the past few decades (McGarr et al., 2002; Foulger et al., 2018; Kivi et al., 2023). The understanding and identification of these types of human-induced earthquakes is crucial in terms of environmental and economic impact, as well as for socio-political and scientific discussion (Gonzalez et al., 2012; Vilarrasa et al., 2019). Recently, the debate over potential induced or triggered nature of cases of felt seismicity has intensified, such as the Oklahoma earthquakes of Mw 5.7 in 2011 and of Mw 5.8 in 2016 (Ellsworth, 2013; Keranen et al., 2013; Yeck et al., 2017), Emilia, Italy, earthquakes of Mw 6.1 and 5.9 in 2012 (Cesca et al., 2013a), Pohang, South Korea, earthquake of Mw 5.5 in 2017 (Grigoli et al., 2018; Kim et al., 2018), Lorca, Spain, earthquake of Mw 5.1 in 2011 (González et al., 2012), and Castor, Spain, earthquake sequence of Mw 4.1 in 2013 (Cesca et al., 2014; Vilarrasa et al., 2021; Vilarrasa et al., 2022), to name a few. Apart from the possibility of injuring people and damaging infrastructure, such earthquakes can have a negative public perception leading to project cancellation (Boyet et al., 2023a).

The first reservoir-triggered seismicity (RTS) case was observed during the filling of Lake Mead at the Hoover Reservoir (US) in the mid-1930s, with ~M4.0 (Carder 1945). Major worldwide RTS cases were detected in the 1960s, such as the M6.1 Hsinenghiang (China) in 1962, Kariba (Zambia) M6.2 in 1963, Kremasta (Greece) M6.3 in 1966, and Koyna (India) M6.3 in 1967 (Gupta, 2002). To date, over 150 RTS cases have been documented (Wilson et al., 2017; Foulger et al., 2018). Studies to understand the triggering mechanisms of RTS show that pore pressure changes in the order of a few tenth of MPa and the associated

54 poroelastic stress changes are sufficient to reactivate deep faults (Rice and Cleary, 1976; Simpson, 1976; Bell

55 and Nur, 1978; Talwani and Acree, 1985; Roeloffs, 1988; Simpson et al., 1988).

56   RTS is generally controlled by the stress state, the geological and hydrogeological properties of the region,

57 and the water-level changes at the reservoir. The perturbation caused by the changes in water-level results in

58 the loading and/or unloading of the subsurface, which may respond in an undrained or drained way. An

59 undrained response leads to an instantaneous pore pressure buildup that is proportional to the height of the

60 reservoir load. In contrast, a drained response leads to pore pressure diffusion into the rock that causes

61 progressive pore pressure build-up as the pressure front propagates into the rock (Table 1). In general, RTS

62 magnitudes are smaller for undrained responses than drained ones (Simpson et al.,1988). The interactions and

63 comprehensive analysis of these two responses are key to understand the causes of RTS cases and eventually

64 improve the forecasting and mitigation of RTS hazard.

65 **Table 1.** The time-distribution types of responses to reservoir-triggered earthquakes (by Simpson, 1988)

Response type	Mechanism	Description	Main features	Cases
Instantaneous response	Instantaneous elastic response and undrained response due to reservoir loading	This type of RTS increases immediately after the initial impoundment of reservoir or changes rapidly after rapid changes in the water level.	Changes in water level have a strong correlation with the change of seismicity, this generally occurs around the reservoir area, and the earthquake magnitude is small, the majority of them are swarm seismicity.	Koyna, Monticello, Manico-3, Nurek, Kariba, Kremesta *Irapé (this paper)*
Delayed response	Increase of pore pressure caused by pressure diffusion through permeable rock below the reservoir	It is only after a period of reservoir impoundment that the seismicity changes continuously	No significant correlation between changes in water level and seismicity, the time delay is obvious, the magnitude is generally large, and the earthquake occurrence point is not limited.	Koyna, Aswan, Oroville

66

67 The RTS cases are booming around the world, with Brazil being one of the concerned countries with 29 RTS

68 cases to date (Sayão et al., 2020). The study of RTS in Brazil started in 1972 with the M3.7 at Carmo do

69 Cajuru reservoir, southeast Brazil (Foulger et al., 2018). The largest recorded event, a M4.2 in 1974, caused

70 damage to several buildings without any fatalities and was associated with nearby reservoirs at Porto

71 Colombia and Volta Grande, both of which started damming in the early 1970s (Sayão et al., 2020).

72 The Irapé dam, located in the state of Minas Gerais, Brazil, is the highest dam in Brazil with about 208 m,

73 and the second highest in South America (França et al., 2010). The Irapé hydropower plant lies in the vicinity

74 of Jequitinhonha River. Seismicity started to increase immediately after the impoundment of the reservoir and

75 completion of the dam with the maximum event of M3.0 occurred on 14 May 2006, coinciding with the peak

76 water level of the dam. The significant magnitude of the earthquake and the early occurrence after-filling of

77 the reservoir impoundment has raised questions about the triggering mechanisms of this RTS. Understanding

78 these mechanisms is crucial for ensuring the safety of infrastructure around the Irapé reservoir and for the

79 local population.

80 In this study, we aim to investigate the potential causes of the main RTS event at Irapé. We initially elaborate

81 on the geological setting and rock characteristics in the vicinity of the reservoir. We explain the characteristics

82 of the RTS at Irapé, including the temporal evolution of the seismicity, which occurred in the short period

83 from December 2005 to May 2006 and the location of the main event based on the local velocity model. Then,

84 we present the performed permeability and porosity tests of cylindrical cores from hard and intact rock

85 samples, which have been extracted near the RTS zone to identify and describe the primary role of porosity

86 and permeability. We perform analytical calculations to estimate the pore pressure and poroelastic stresses in

87 response to the highest water level of the reservoir filling and the time it would take for the pore pressure

88 diffusion front to reach the depth of the main event. We present evidence that the cause of RTS at Irapé was

89 the undrained response of the subsurface to reservoir impoundment.

90 **2. Geological setting and RTS at Irapé**

91 **2.1 Geological setting**

92 The area of Irapé is located within the domain of the Pre-Folding Belt Cambrian Araçuaí, which is oriented

93 approximately in a north-south direction and defines the eastern part of the São Francisco Craton in the State

94 of Minas Gerais (Almeida, 1977). Approximately 80% of the reservoir area in Irapé corresponds to the

95 Chapada Acauã Formation. The Chapada Acauã Formation, which has been investigated near the Irapé Shear

96 Zone (Araujo et al., 2010), consists of carbonaceous mica-schist rocks, locally with pyrite, garnet, or graphite

97 (Lima, 2002). This rock is intensely deformed, characterized by the formation and rotation of quartz sub-

98 grains and the migration of grain edges (Araujo et al., 2010). It This formation is characterized by typical

99 passive margin sedimentation and is associated with sediment deposition in the Macaúbas Basin along with

100 the Nova Aurora Formation (Silva et al., 2014). To the east of the Chapada Acauã formation, The Ribeirão da

101 Folha Formation is found to the east of the Chapada Acauã formation, consisting of mica shales, quartzite,

102 and cal-silicates rock (Figure 1).

103

104
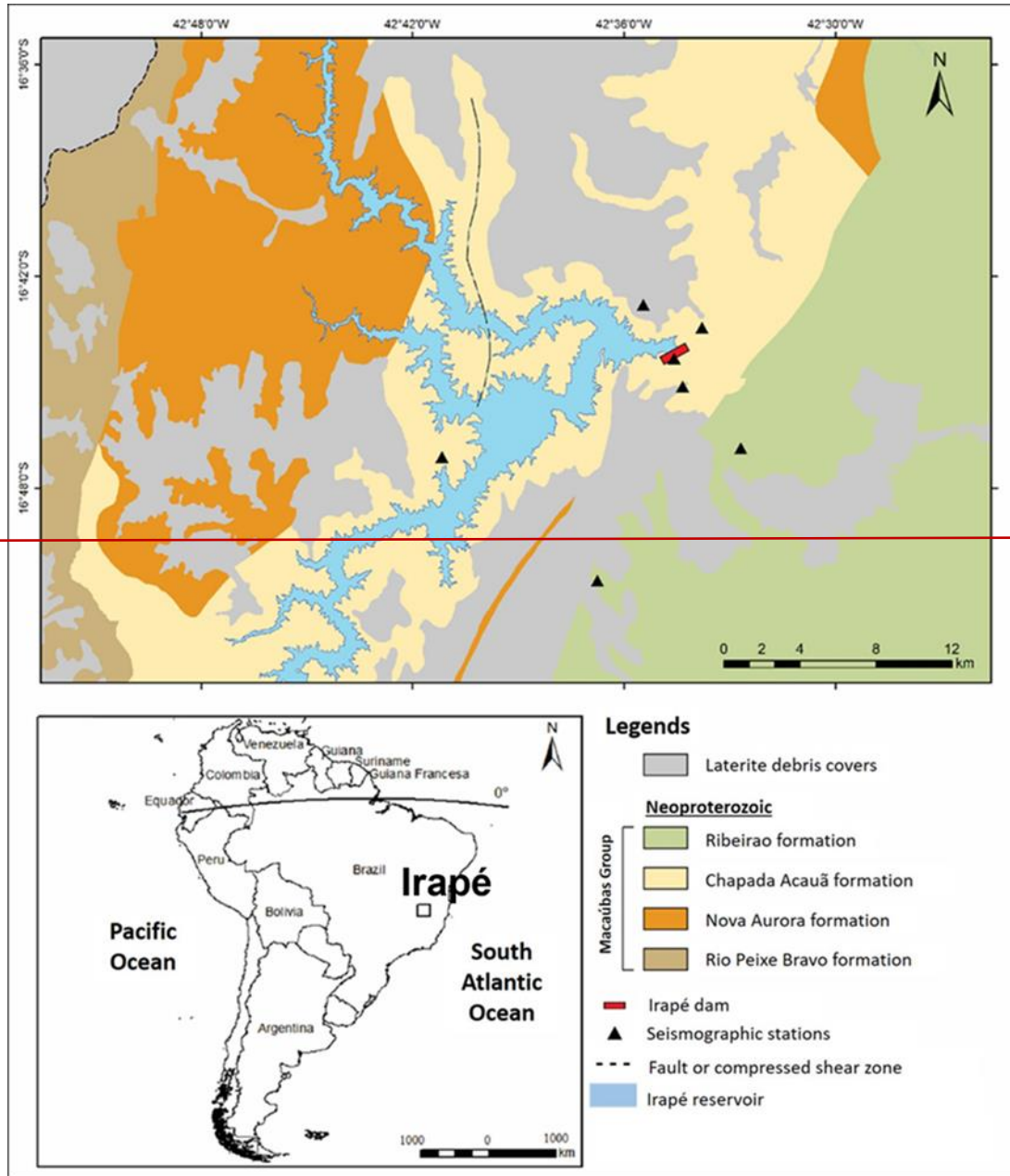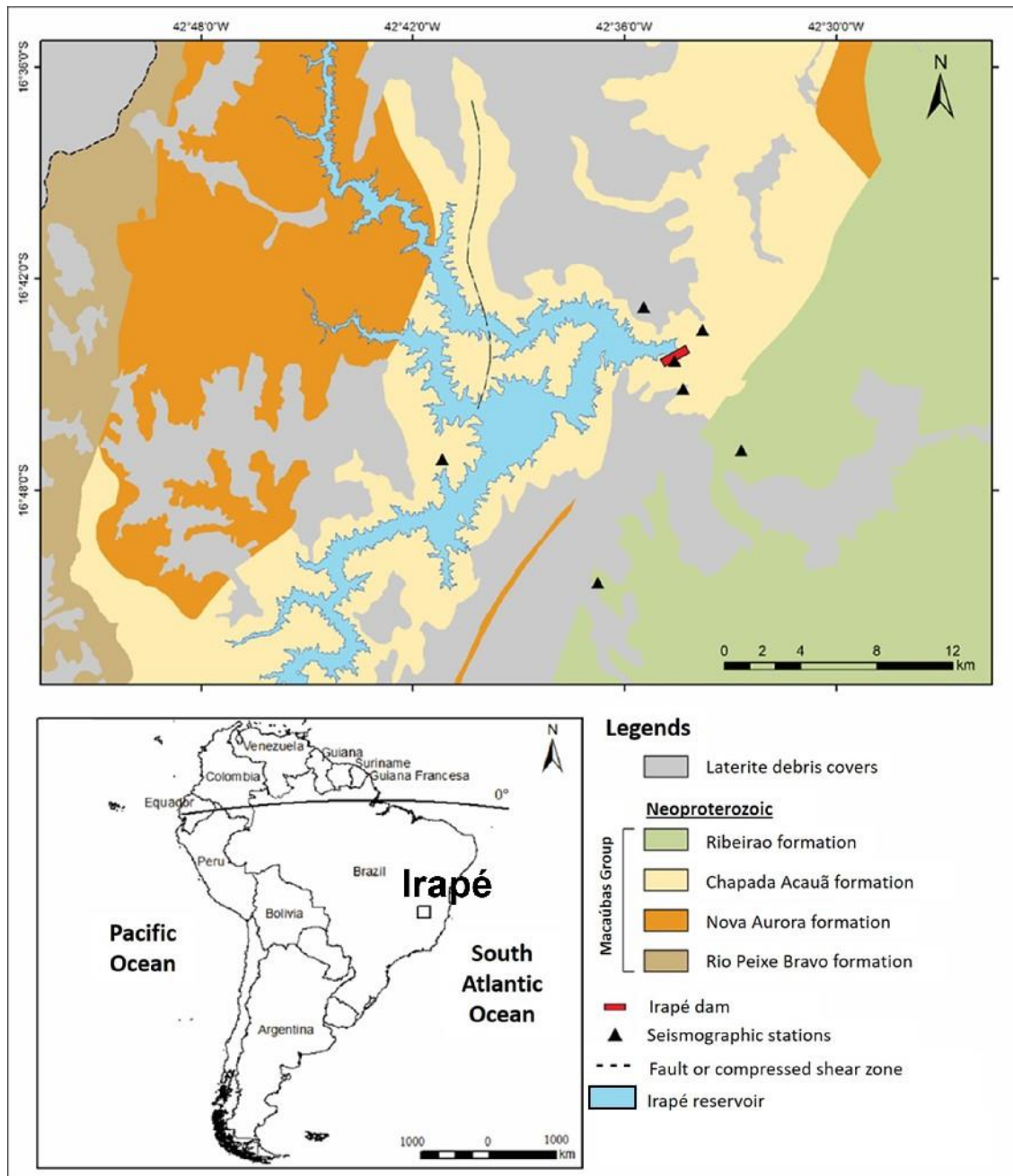
Figure 1. Geological map of Irapé reservoir and surrounding area

2.2 Background on the reservoir-triggered seismicity at Irapé

The Irapé reservoir covers an area of 137.8 km^2 with a reservoir volume of 5.964 km^3. The dam was constructed on the Jequitinhonha River, filling the reservoir to a maximum height of 137 meters (Figure 1 and Table 2). The dam area was monitored by a three-component seismic network at three stations prior to three

110 ~~3~~ years of its impoundment, which started on 7 December 2005. These stations did not detect any seismicity

111 before the impoundment (Chimpliganond et al., 2007).

112 **Table 2.** Characteristics of the main RTS event at Irapé (França et al., 2010)

Dam height (m)	Length (m)	Volume (km³)	Max. reservoir water depth (m)	Reservoir area (km²)	Seismicity type	Date	Magnitude (mR)	Io (MMI)	ΔT(yr)
208	540	5.964	137	137.8	Initial	14 May 2006	3.0	III-IV	0.5

113 *ΔT: interval time (years) since the start of filling/impoundment; MMI: modified Mercalli Intensity*
114 *scale, mR: magnitude Regional.*

115 Microearthquakes started to be detected just one day after the impoundment began, exceeding 300

116 microearthquakes by October 2006. The largest event occurred on 14 May 2006 with a M3.0 that was felt at

117 the reservoir area at a depth of 3.88 km (Chimpliganond et al., 2007; França et al., 2010). The seismicity

118 occurred within a small area, with epicentres in the lake and its nearby margins (less than 3 km from the

119 narrow lake), close to the dam axis. The epicenters are distributed from 0 to 11.4-km depth, showing a

120 progressive increase in depth (see Table S1). The evident temporal correlation between the start of the

121 reservoir impoundment and the occurrence of seismicity leads us to investigate a causative relationship

122 (Figures 2 and 3). The spatial distribution of the epicentres also suggests the hypothesis that this is another

123 case of RTS of the initial response type.
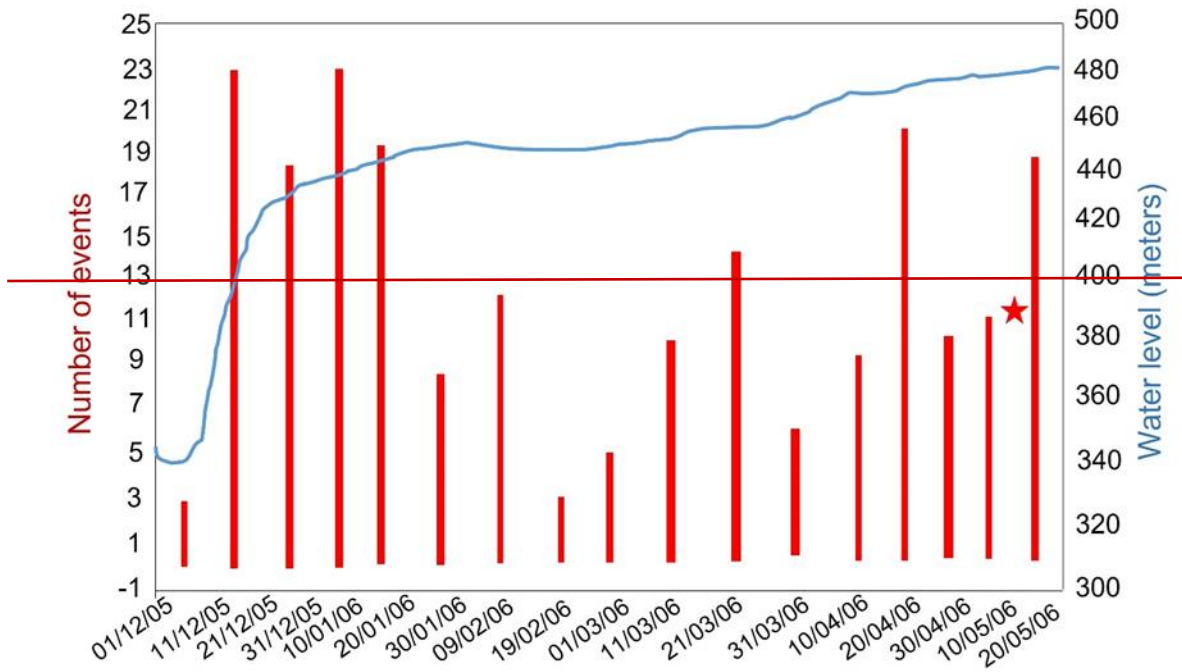
124

125

126
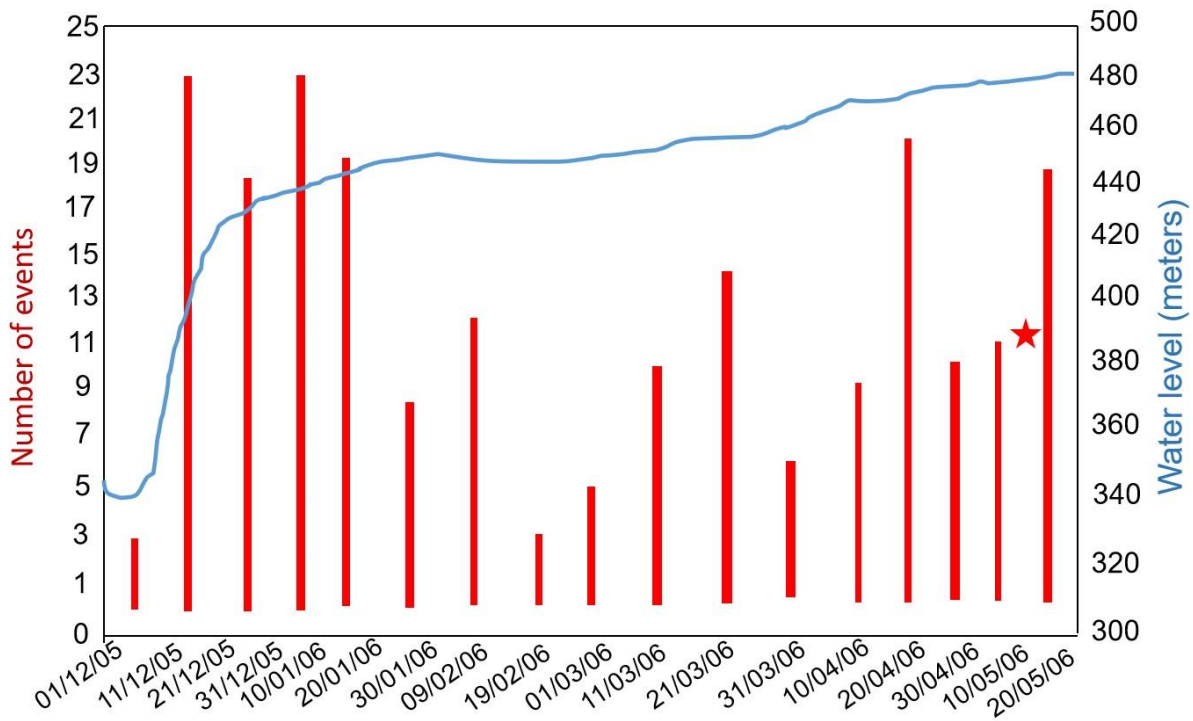
127

128 **Figure 2**. Temporal evolution of RTS at Irapé by ten days. Number of events during December 2005 to May

129 2006 (histogram) at Irapé and average water elevation above the mean sea level (blue line) are illustrated. The

130 red star indicates the time when the main and largest event occurred, M3.0 on 14 May 2006 (modified from

131 Silva et al., 2014).

132   The events were analysed using the program Seismic Analysis Code (Goldstein and Snoke, 2005), in which

133 the arrival of the P and S waves and the polarity are considered. The hypocentre location of the events that

134 were recorded by three stations was computed with the program HYPO71 (Lee and Lahr, 1975). The analysis

135 of seismograms went through a double-checks routine (Silva et al., 2014). The local monitoring station

136 presented operational challenges, which resulted in positional uncertainty of seismic events (Silva et al.,

137 2014). The velocity model that was used to locate the seismic events was based on a deep seismic refraction

138 survey in combination with local geological interpretations and studies of the crustal structure in south-eastern

139 Brazil (Assumpçao et al., 2002b).
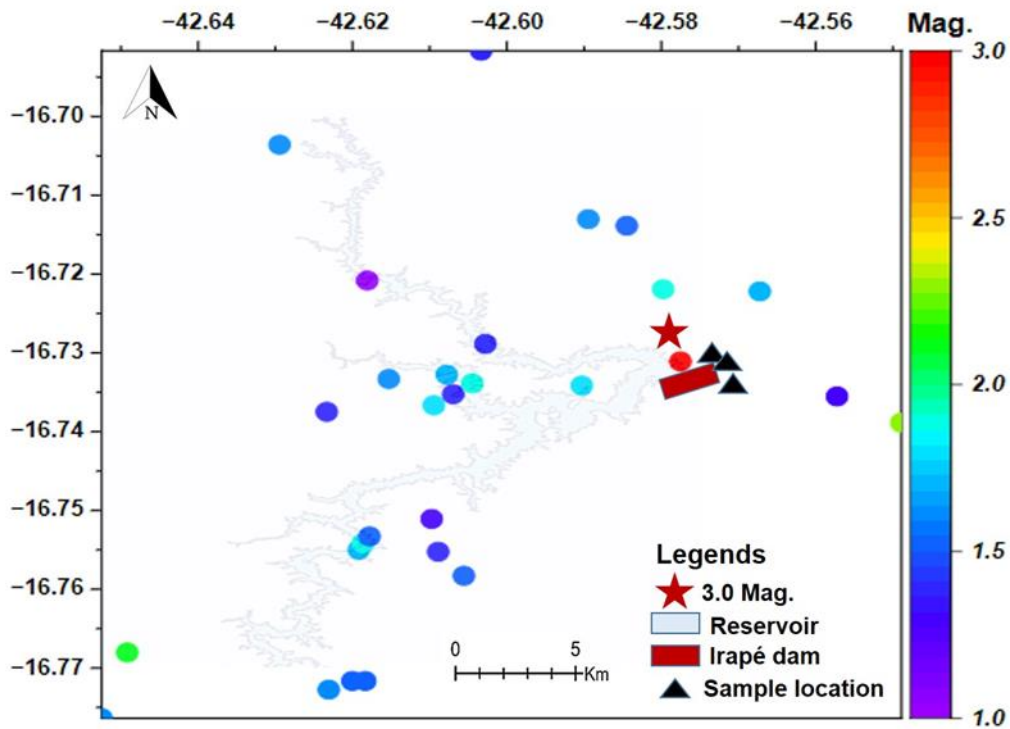
140

141 **Figure 3.** RTS Distribution in the initial period with location and magnitude (see colour scale), the red star is

142 the main event felt near the dam and black triangles denote the samples location.

143   Velocity models were adopted based on a deep seismic refraction survey in combination with local

144   geological interpretations and studies of the crustal structure in south-eastern Brazil to locate seismic events

145   in the Irapé area (Assumpção et al., 2012). The local velocity model consists of a superficial 4.8 km-thick

146   layer with a P-wave velocity (V_p) of 4.5 km/s, representing the mica-schist to graphite-schist rocks from

147   surface, and a second layer from schist to crystalline basement rocks with a thickness of 11.2 km with P-wave

148   velocity (V_p) of 6 km/s (Marshak et al., 2006; Silva et al., 2014).

149   The repetition of a structural trend in the NE-SW direction originates from the geological and geophysical

150   structuring of the crust (Silva et al., 2014). The stress regime in the Irapé region has been estimated to be a

151   normal faulting stress regime. The accuracy of the focal mechanisms remains a subject of debate due to the

152   low quality of the seismic data recorded by analogue seismograms and uncertainties associated with the

153   velocity model. Consequently, the focal mechanisms of the May 14, 2006, M3.0 earthquake have not been

154   resolved yet (Silva et al., 2014).

155   **3.Materials and methodology**

156   We inspected the Irapé site and surrounding areas as well as the outcrops. The dam area is surrounded by

157   mica-schist rock, which is shiny, ranging from blackish to medium grey in colour, with foliated, fine to

158   medium-grained textures. According to the local velocity model, there is a superficial layer that is 4.8-km

159   thick, representing mica-schist to graphite-schist rocks at the surface. Below that, there is a second layer that

160   is 11.2-km thick, consisting of crystalline basement rock. Measurements from these samples are crucial for

161   understanding the estimated permeability beneath the subsurface in the context of the main event, which

162   occurred at a depth of 3.88 km (França et al., 2010). Since the epicenter of the main event was located about

163   1 km away from the dam, we collected bulk rock samples from different locations around the dam, as well as

164   nearby outcrops, by digging pits that were 0.10-m deep.

165   **3.1 Laboratory experiments**

166   We have extracted cylindrical core samples perpendicular to the bedding planes of mica-schist rock. We

167   have performed tests on three sets of samples, with a total of 11 core samples, of hard and intact samples

168   because the rest of the samples were fragile and fractured during the coring from bulk samples (Table 3). The

169   retrieved cylindrical plugs have a length ranging from 3.8 to 5.0 cm and a diameter of 2.50 cm, which meets

170   the International standard criteria (Core Lab) to measure core plug samples by Ultra-Pore 300 and Ultra-Perm

171   610 (Figures 4).

172
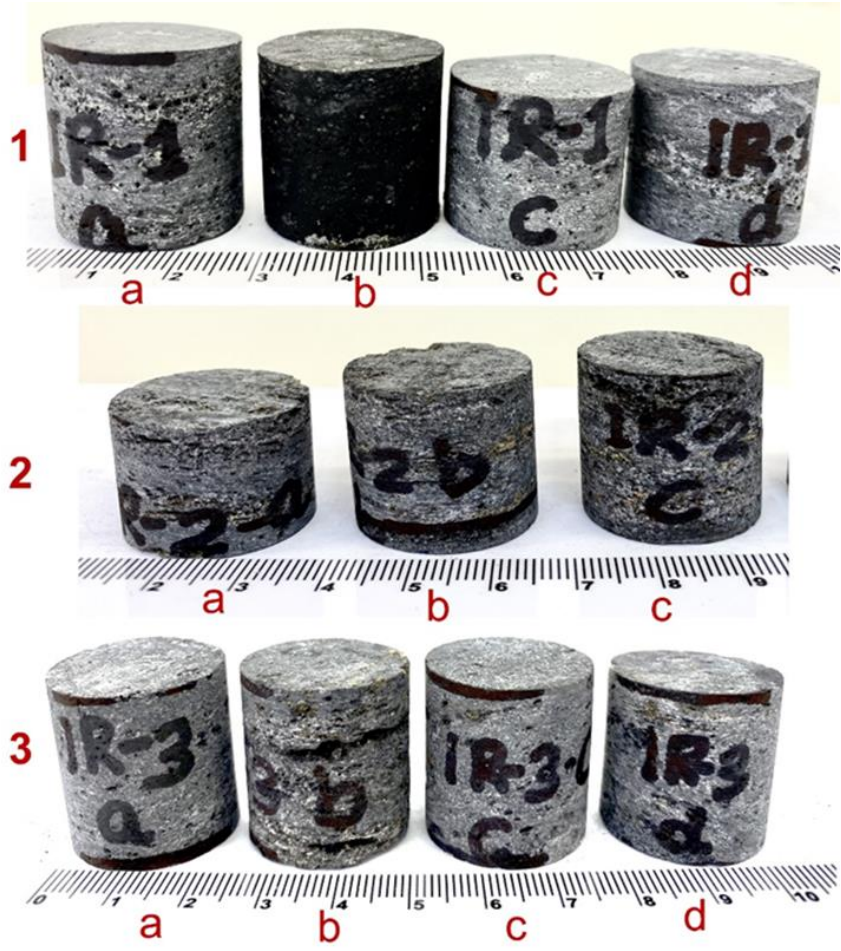
173

174   **Figure 4.** The three sets of mica-schist rock samples (1, 2, and 3) after cylindrical coring from bulk samples

175   (⊥ coring of cylindrical plugs has been done by loading perpendicular to the bedding planes).

176   We conduct porosity measurements using the Ultra-Pore 300, which is manufactured by Core Lab Instruments

177   in Texas, USA. The Ultra-Pore 300 is a gas expansion helium pycnometer specifically designed for

178   determining the grain volume or pore volume of both core plug and full-diameter samples. To achieve this,

179   we utilized matrix cups designed for samples with diameters ranging from 2.5 to 3.8 cm, equipped with a

180   Setra 204 transducer rated for pressures ranging from 0 to 1.72 MPa. We determined the pore volume using

181   the nitrogen gas (N_2) expansion technique (API,1998; Ceia et al., 2019).

182   We measure the intrinsic permeability of rock samples using Ultra-Perm 610 Permeameter. This precision

183   equipment, which controls backpressure, maintains a constant rate or mean pressure at 0.69 MPa. Before

184   testing, samples are cleaned with soxhlet equipment and toluene, followed by drying in an oven. The

185   permeability measurements included a permeameter, nitrogen source, stopwatch, a core holder, a bubble tube,

186   and a digital calliper. The core holder is pressurized to 3.45 MPa confining pressure using compressed air.

187   The bubbles passing through a burette are timed, and outflow gas volume is recorded. The permeability is

188   calculated using Darcy's law, considering core dimensions. Hard rock core samples, like mica-schist, require

189   long stabilization times due to the low permeability.

190   **3.2 Analytical calculations of undrained pore pressure and stress changes**

191   Reservoir impoundment causes an undrained effect in the subsurface that manifests as ~~an~~ instantaneous pore

192   pressure and stress changes below the reservoir (Skempton, 1954). The change in the vertical stress, $\Delta\sigma_v$,

193   equals the weight of the water level rise assuming an extensive reservoir. The horizontal stress, assuming

194   oedometric conditions, changes because of the increase in the vertical stress and ~~proportionally to~~ the un-

195   drained pore pressure change~~s~~ as (Rutqvist, 2012)

196    $$\Delta\sigma_h = \alpha\frac{(1-2v)}{(1-v)}\Delta p\,, \tag{1}$$

197

198    $$\Delta\sigma_h = \frac{v}{(1-v)}(\Delta\sigma_v) + \alpha\frac{(1-2v)}{(1-v)}\Delta p \tag{1}$$

191 where $\Delta\sigma_h$ is the horizontal stress change, α is Biot's coefficient, ν is Poisson's ratio and Δp is the pore

192 pressure change. Additionally, in an isotropic and homogeneous poroelastic material subject to un-

193 drained conditions, the change in pore pressure resulting from a change in stress can be computed as

194 (e.g., Rice and Cleary, 1976; Cocco and Rice, 2002)

195
$$\Delta p = \frac{B}{3}\Delta\sigma_{kk},\tag{2}$$

196 where $\Delta\sigma_{kk} = \Delta\sigma_v + 2\Delta\sigma_h$, $\Delta\sigma_{kk}$ is the mean stress change and B is the Skempton's coefficient of

197 mica-schist rock (Roeloffs, 1988). Here we adopt the sign criterion of geomechanics, i.e., compressive

198 stresses are positive. Equations (1) and (2) constitute a system of two equations with two unknowns. Its

199 resolution yields the undrained pore pressure change as

200
$$\Delta p = \frac{B}{3}\frac{\Delta\sigma_v}{\left(1 - \frac{2B\alpha(1-2\nu)}{3}\frac{}{(1-\nu)}\right)}.\tag{3}$$

201

202
$$\Delta p = \frac{B}{3}\frac{(1+\nu)\Delta\sigma_v}{\left(1 - \nu - \frac{2B}{3}(\alpha - \nu - 2\alpha\nu)\right)}.\tag{3}$$

203 **3.3 Analytical calculations of the time at which the pore pressure diffusion front reaches the**

204 **depth of the earthquake**

205 The advancement of the pore pressure front within the subsurface is controlled by diffusivity

206
$$D = \frac{k\rho g}{\mu S_s}\tag{4}$$

207 where, D is diffusivity, k is the intrinsic permeability, ρ is water density, g is gravity, μ is water viscosity,

208 and S_s is the specific storage coefficient. The time at which the pore pressure front reaches a certain

209 distance r is given by

210
$$t = \frac{r^2}{D}\tag{5}$$

211 **4.Results**

212   **4.1 Porosity and permeability measurements**

213   The results of our laboratory measurements are provided in Table 3. These data are subject to meas-

214   urement uncertainties inherent to the experimental equipment used according to the standard procedure.

215   Laboratory measurements of samples of mica-schist reveal a low permeability (Table 3 and Figure 6).

216   The maximum permeability is 0.0098 mD, but most of the samples present a permeability lowest meas-

217   urable value of the apparatus, i.e., ~~lower than~~ 0.002 mD. Such permeability is in the range of low-

218   permeability rock, which act as a barrier to flow. Most of the samples have a porosity between 6 to

219   10%, except for two with higher porosity. The low permeability of mica-schist could be explained by

220   the fact that the larger pores are not well connected (Figure 5). In general, there is no correlation between

221   permeability and porosity (Figure 6).
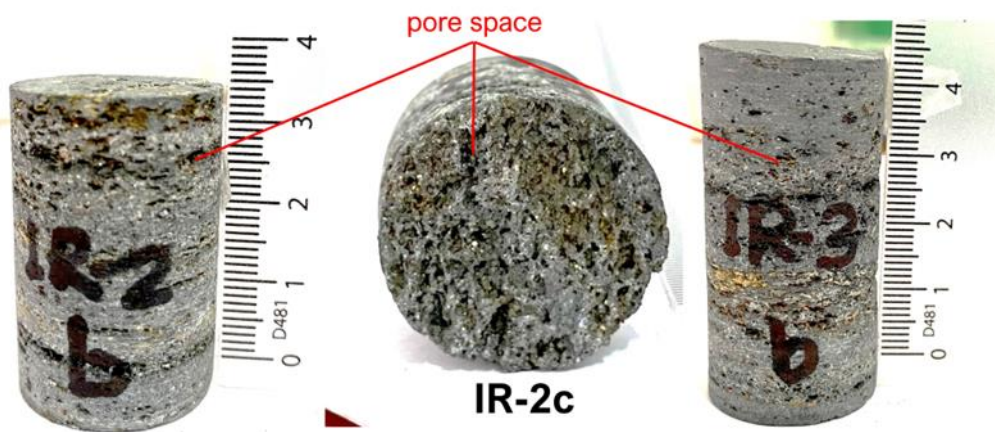
222

223   **Figure 5.** Megascopic representation of samples IR-2 b, c, and IR-3b showing pores that are not well-

224   connected.

225   **Table 3.** Location of samples with permeability and porosity data from measured cores

226

Location (lat., long.)	Sample Numbers	Permeability (mD)	Porosity (%)
16.73872, 42.57680	IR-1a	<0.002	7.5
	IR-1b	<0.002	6.8
	IR-1c	<0.002	8.8
	IR-1d	0.0098	6.6
16.74038, 42.57652	IR-2a	<0.002	9.5
	IR-2b	0.0038	10.5
	IR-2c	0.0038	14.7
16.72438, 42.56316	IR-3a	<0.002	6.9
	IR-3b	<0.002	13.3
	IR-3c	<0.002	7.1
	IR-3d	<0.002	6.3

227   *Experiments loaded perpendicular to bedding plane ($\perp$)*

228

229
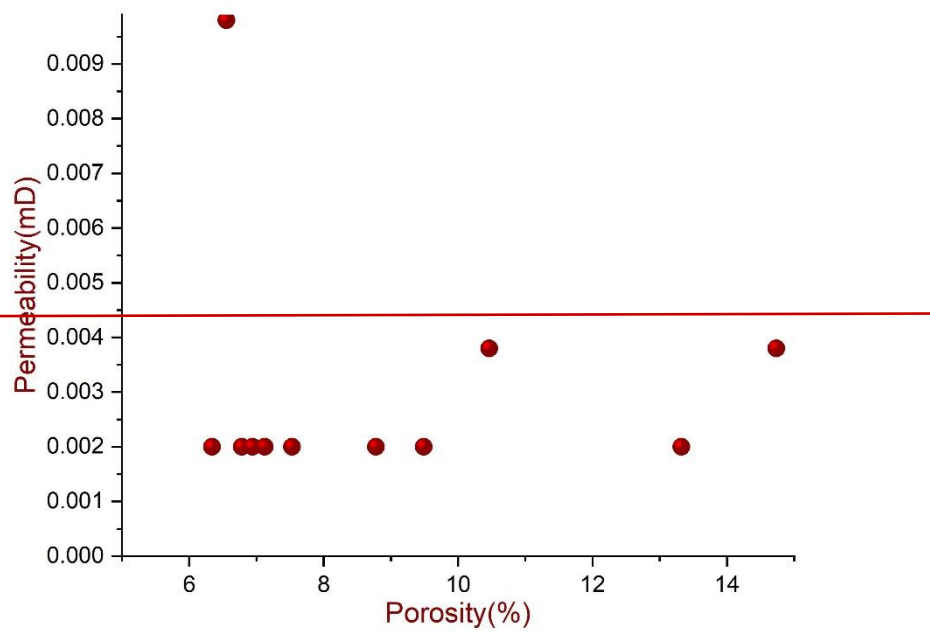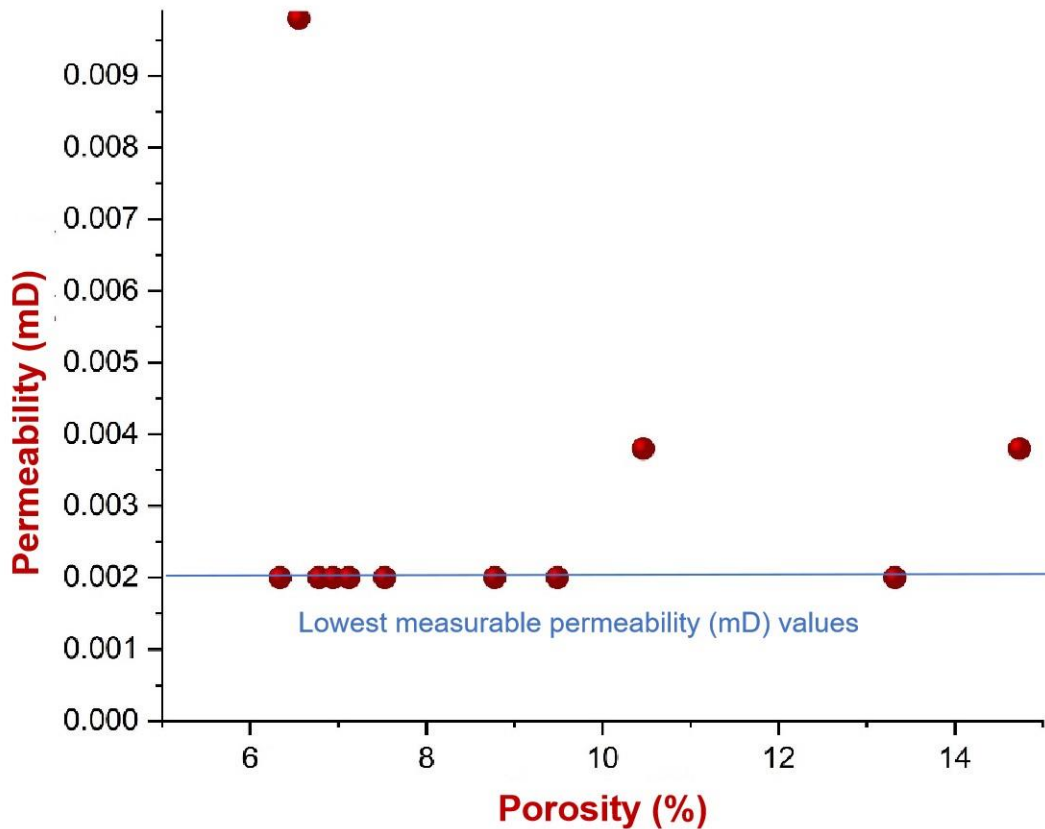
Figure 6. Porosity-permeability relation of mica-schist rock samples.

4.2 Undrained response of rock: changes in pore pressure and stress

The 136 m of water level increase at the time of the M3.0 earthquake resulted in an increase in the vertical stress of 1.36 MPa. To compute the pore pressure change caused by the reservoir impoundment, the Biot coefficient, Skempton's B coefficient and Poisson's ratio of mica-schist are needed (Eq. (3)). Since such measurements are not available, we adopt the values of Opalinus Clay because it is a similar rock to mica-schist (both are shales primarily composed of quartz minerals). Thus, we assume Skempton's B coefficient of 0.92, undrained Poisson's ratio of 0.39 and Biot's coefficient of 1. With these values, the resulting pore pressure change is ~~0.54~~ 0.61 MPa. Consequently, the horizontal stress change is of ~~0.~~1.09 MPa (Eq. (1)). These pore pressure and stress changes result in an increase in the vertical effective stress of ~~0.82~~ 0.75 MPa and ~~a~~ in the horizontal effective stress ~~decrease~~ of 0.48 MPa, increasing the deviatoric stress in more than ~~1~~ 0.25 MPa.

4.3 Pressure diffusion along mica-schist

243   The measured intrinsic permeability of mica-schist is in the order of 10^{-18} m^2 (Table 3). Assuming a

244   specific storage coefficient in the order of 1.05×10^{-6} m^{-1}, diffusivity (Eq. (4)) results in 9.5×10^{-6} m^2/s.

245   Taking into account that the depth of the M3.0 earthquake occurred at 3.8 km, the time at which the

246   pore pressure front would reach this depth by diffusion (Eq. (5)) is in the order of 50,000 years by

247   assuming the absence of fractures.

5.Discussion

249   RTS has been the focus of many studies, but the origin and development of RTS are still unclear in

250   many cases (Gupta et al., 2016; Arora et al., 2018). There is a general consensus that there are two main

251   triggering mechanisms (Simpson et al., 1988). On the one hand, low-permeability rock has an undrained

252   response to the water-level changes of the reservoir, which acts as a loading, instantaneously increasing

253   pore pressure and causing poroelastic stress changes deep underground (Chen and Talwani, 2001;

254   Vilarrasa et al., 2022; Raza et al., 2023). On the other hand, in the presence of permeable rock or a

255   permeable fracture network, pore pressure diffuses downwards, which may eventually trigger an

256   earthquake if a critically stressed fault becomes pressurized (Talwani and Acree, 1985).

257   At Irapé, the low-permeability of the rock below the reservoir, i.e., mica-schist with permeability in

258   the order of 10^{-18} m^2 or lower, hinders pore pressure diffusion. Given that the hypocentre was located at

259   3.88 km depth, the pressure propagation front would take in the order of 50,000 years to start

260   pressurizing the depth at which the earthquake was nucleated. Even assuming that the presence of

261   fractures enhanced the rock permeability by three orders of magnitude, which would be the upper limit

262   of observed permeability enhancement of low-permeability rock at the field scale (Neuzil, 1986), the

263   pressure front would take 50 years to reach 3.88 km depth. The permeability enhancement due to the

264   presence of fractures could become larger in crystalline than in clay-rich rock, reaching an increase of

265   up to five orders of magnitude (Bondarenko et al., 2022). Such high permeability enhancement caused

266   by fractures is not feasible in clay-rich rock like mica-schist because of its ductility and low dilatancy

267   angle, which prevents fractures from becoming open pathways. At Irapé, the necessary permeability of

268   the rock to reach the depth of the largest earthquake within 0.5 years, i.e., the delay of the earthquake

269   with respect to the start of impoundment, would be of 10^{-13} m^2, five orders of magnitude higher than

270 the actual permeability of mica-schist. Such high permeability enhancement is deemed unlikely for

271 mica-schist.

272 Considering the load caused by the water-level rise in the reservoir of 136 m, the low-permeability

273 mica-schist experienced an undrained response, with subsequent poroelastic stress and pore water

274 changes. We have estimated these changes analytically, finding a vertical effective stress increase of

275 ~~0.82~~ 0.75 MPa, a horizontal effective stress increase of 0.48 MPa, and a pore pressure increase of ~~0.54~~

276 0.61 MPa. Given the normal faulting stress regime at Irapé, these changes cause an increase in the

277 deviatoric stress that could destabilize faults in the subsurface. These changes in pore pressure and stress

278 levels provide valuable insights into the dynamic behaviour of the geological formation and are crucial

279 considerations in understanding the reservoir response to alterations in reservoir water levels. We

280 contend that the rapid loading of the reservoir weakens this fault because of the undrained stress and

281 pore pressure changes (Figure 7).

282 In addition, the megascopic representation of core samples in the configuration of the physical

283 evidence illustrates that rock can exhibit relatively high porosities and low permeability when their

284 pores are not well-connected (Figure 5). Thus, mica-schist may present preferential lateral fluid

285 migration at depth, following the foliation direction. The surface rock beneath the Irapé reservoir is

286 highly metamorphosed and despite having high porosity, the rock presents low permeability. Therefore,

287 pore pressure diffusion is disregarded as the potential cause triggering the seismicity at Irapé.

288

289
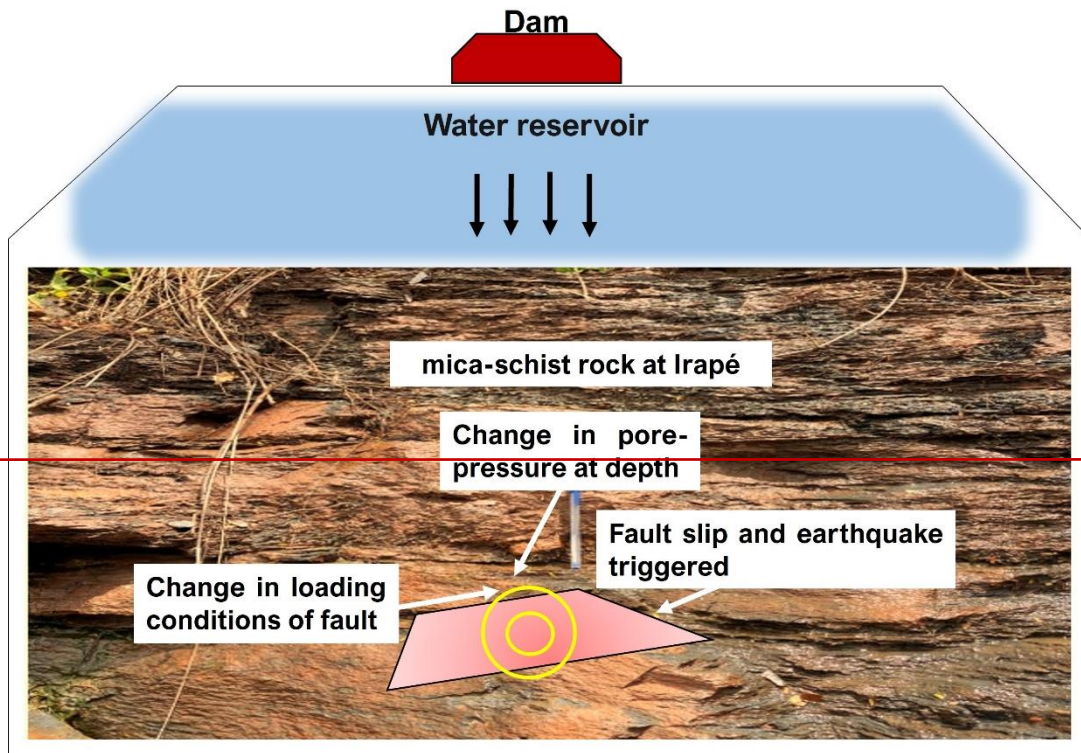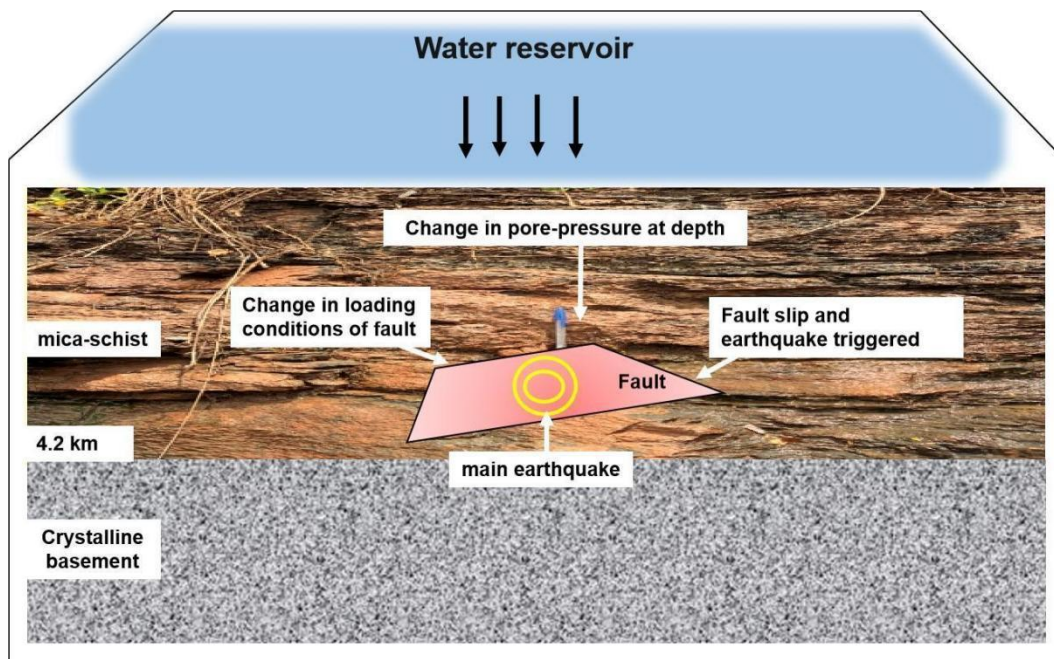
Figure 7. Schematic description of the mechanism of RTS at Irapé, indicating the effect of the weight of the reservoir water volume due to undrained response in low-permeable mica-schist rock (the background photo was taken in the field from an outcrop at Irapé).

The regional geology at the eastern part of the São Francisco Craton in the State of Minas Gerais follows a N-S direction (Almeida, 1977). Silva et al. (2014) also mentioned that the repetition of a structural trend in the NE-SW direction originates from the geological and geophysical structuring of the crust. This trend makes it feasible to assume the existence of a N-S vertical mature fault that could become destabilized by small changes in the effective stress. An association of such seismicity with the shear zone along reservoir /lineaments suggests the reactivation of such faults under the influence of reservoir impoundment.

Mitigation of the risk of RTS requires knowledge of the physical mechanisms that may trigger seismicity. Thus, ~~it is crucial to~~ a thorough~~ly~~ characterization of the site ~~by~~ to measure rock physical properties is crucial. Analytical and numerical solutions should integrate the physics of the problem, ~~such as~~ in particular, poromechanics to assess both the undrained response of the subsurface to reservoir impoundment and pore-pressure diffusion. Such models should include the rock layers below the reservoir down to the crystalline basement and their characteristics, including features like faults. Before the construction of the dam, the hazard of triggering moderate to large earthquakes should be estimated, to disregard locations with high probability of RTS. This estimation requires knowing the hydro-mechanical properties of the rock layers, i.e., permeability, porosity, stiffness, and strength, as well as the design parameters of the dam, i.e., height for potential future projects. Note that at Irapé, the porosity and permeability measurements have not been done until now, but should have been done prior to the design of the dam. The successful management of RTS requires an interdisciplinary approach combining concepts of hydrogeology, geomechanics and seismology.

~~Finally, to address and manage RTS risks, the traffic light protocol (TLP) is being employed. In general, TLP initiates the green light as the primary approach allowing operations without restrictions, the yellow light as the point to activate mitigation measures, and the red light as the point necessitating regulatory intervention. The efforts have also begun by linking the configuration of TLPs with risk-oriented measures, infrastructure harm, and the likelihood of loss or damages while adapting them to real-time data. The occurrences that may ensure after an operation are crucial, given their substantial impact on standard risk management. Nevertheless, these methodologies can be revolved around by assessment~~

320 ~~of events succeeding in the conclusion of an operation. The utilization of physics-based models holds~~

321 ~~promising by illustrating and projecting anticipated seismic activity, enabling the anticipation of future~~

322 ~~warnings and risks, and build up the information for operational adjustments and for future mitigation~~

323 ~~(Boyet et al., 2023b) (Figure 8).~~

324 To address and manage RTS risks, the Traffic Light Protocol (TLP) should be employed (Figure 8). A

325 TLP is a tool that assists decision makers to decide how to operate the dam to minimize risks. The TLP

326 has three levels of operation: (1) a green light that allows operations to proceed without restrictions, (2)

327 a yellow light that requires to activate mitigation measures, and (3) a red light that urges to stop opera-

328 tion Efforts have been made regarding the incorporation of real-time data with the application risk-

329 oriented measures to prevent infrastructure damage and nuisance to the local community. Incorporating

330 in TLP the two types of RTS, i.e., immediate events induced by the undrained response of the subsurface

331 to water-level changes, and delayed seismicity induced by pore pressure diffusion, is crucial. To this

332 end, the utilization of physics-based models is promising since they are capable of anticipating seismic

333 activity, enabling operational adjustments for future mitigation of RTS risk (Boyet et al., 2023b) (Figure

334 8).
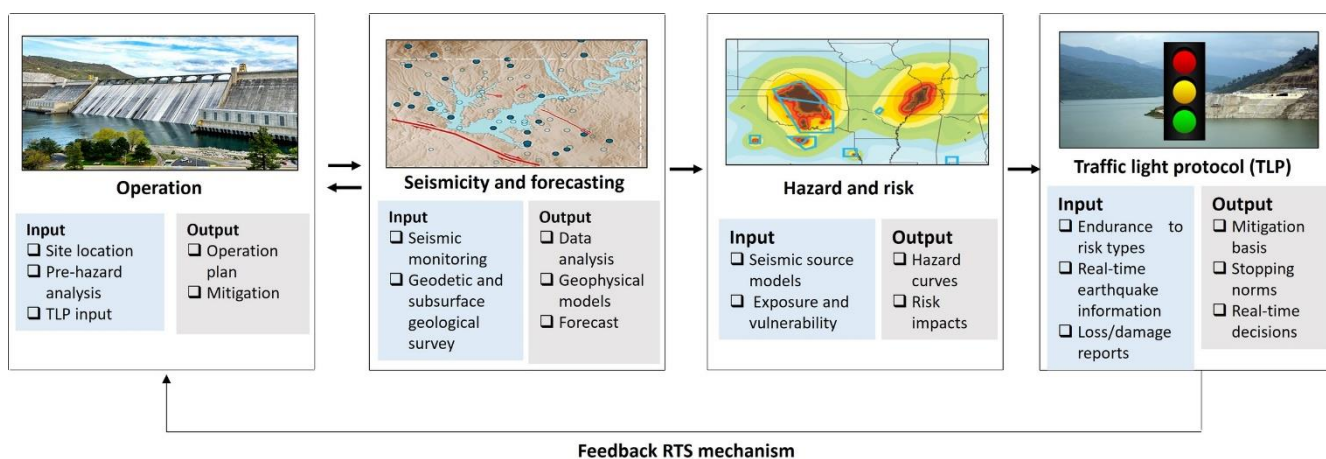
335

336

337 **Figure 8.** Reservoir operations and impoundment are strategically designed to reduce the risk of RTS.

338 Monitoring seismic and geophysical activities yields information for predictive earthquake models. The

339 catalogues of earthquakes and source/origin models are applicable in the assessment of hazard and risk.

340 These assessments of risk and hazard can guide the development of a traffic light protocol (TLP), func-

341 tioning as a dynamic decision module during operations. The display of each box shows the classifica-

342 tions of input data (blue boxes) and output results (grey boxes).

343 Regarding the mitigation approaches for RTS within the framework of a TLP, the effectiveness of an

344 operator heavily relies on the efficiency of mitigation strategies implemented at the yellow-light stage.

345 Ideally, these strategies would proficiently diminish seismic risks and hazards, ultimately circumvent-

346 ing the red-light scenario that terminates the operation. Thus, TLPs can be one major strategy and strong

347 decision-making tool for operators to minimize the risk of RTS for future developments of dams.

348 **6.Conclusions**

349 We have analysed RTS at Irapé to discern the cause of the triggered seismicity. The measured low

350 permeability of the rock at Irapé disregards pore pressure diffusion as the triggering mechanism and

351 suggests that the M3.0 RTS was triggered by the undrained response of the subsurface to reservoir

352 impoundment. Analytical calculations estimate that pore pressure increased by ~~0.54~~ 0.61 MPa in

353 response to an increase of 136 m in the reservoir-water level. The resulting vertical effective stress

354 increased by 0.75 ~~0.82~~ MPa and the horizontal effective stress ~~decreased~~ by ~~0.34~~ 0.48 MPa. Thus, the

355 deviatoric stress would increase in a normal faulting stress regime, like the one at Irapé, destabilizing

356 the fault and causing RTS. Both laboratory measurements and analytical calculations support the

357 hypothesis that the initial seismicity was triggered by the undrained response of the subsurface to the

358 loading of the reservoir at Irapé. This study ~~also~~ suggests that the occurrence of such earthquakes may

359 be avoided by thorough site characterization and carefully ~~manipulating~~ management of the reservoir

360 loading following TLPs that mitigate RTS risk.

361 **Data availability**

362 The data analysed and /or used in this study are presented in the Supplementary Material.

363 **Supplementary Material**

364 The Supplementary Material related to this article is available online.

Author contributions

H.R., G.S.F., V.V. co-designed the study. E.S. and H.R. did sample and provided map. H.R. wrote the paper performed laboratory measurements. H.R. and V.V. did the analytical calculations. All authors reviewed, contributed to the interpretation of the results, and edited the paper.

Competing interests

The corresponding and co-authors state that there are no competing interests.

Acknowledgments

This study was financed in part by the Coordenação de Aperfeiçoamento de Pessoal de Nível Superior -Brasil (CAPES) -Finance Code 001. The authors acknowledge funding from the Spanish National Research Council (CSIC) under the Program for Scientific Cooperation iCOOP+ through the Project COOPA20414. V.V. acknowledges funding from the European Research Council (ERC) under the European Union's Horizon 2020 Research and Innovation Program through the Starting Grant GEoREST (www.georest.eu) under Grant agreement No. 801809. IMEDEA is an accredited "Maria de Maeztu excellence Unit" (Grant CEX2021-001198, funded by MICIU/AEI/ 10.13039/501100011033). G.S.F gratefully acknowledges CNPq (Grant 310240/2020-4 PQ-1C). G.S.F., H.R. and E.S. also thank to INCTET-CNPq (Institutos Nacionais de Ciência e Tecnología de estudos tectónicos) Brazil. We thank to Prof. Carlos Jorge de Abreu for conducting samples measurements at Laboratory of Physical Properties of Rocks at the University of Brasília.

References

Almeida FFM, The São Francisco Craton. Brazilian Journal of Geosciences,7:349-364,1977

API, 1998. Recommend Practices for Core Analysis. RP40. American Petroleum Institute. 2nd Edition.

Araujo Filho, J. O; Silva, G. F; Lima, E. A. M; Ferreiara, V. N; Batista, O. C. A; Franca, G. S. Mapeamento Geoestrutural da área de influência da Usina Hidrelétrica de Irapé, Grão Mogol, MG. Anais do 45º Congresso Brasileiro de Geologia, Sociedade Brasileira de Geologia, 2010.

389 Arora, K., Srinu, Y., Gopinadh, D., Chadha, R.K., Raza, H., Mikhailov, V., Ponomarev, A., Kiseleva, E.
390   and Smirnov, V. Lineaments in Deccan Basalts: The Basement Connection in the Koyna–Warna
391   RTS Region. Bull. Seismol. Soc. Amer., v.108 (5), DOI: 10.1785/0120180011, 2018.

392 Assumpçao, M., James, D., & Snoke, A., Crustal thicknesses in SE Brazilian Shield by receiver function
393   analysis: Implications for isostatic compensation. J. Geophys. Res., 107(B1). ,2002b

394 Assumpção, M; Feng, M; Tassara, A; Julia, J., Models of crustal thickness for South America from
395   seismic refraction, receiver functions and surface wave tomography. Tectonophysics, 609:82-
396   96, 2012.

397 Bell, M.L., Nur, A., Strength changes due to reservoir-induced pore pressure, stresses, and application
398   to Lake Oro-Berrocal. J. Geophys. Res. 83, 4469–4483, 1978.

399 Bondarenko, N., Podladchikov, Y. & Makhnenko, R. Hydromechanical impact of basement rock on
400   injection-induced   seismicity   in   Illinois   Basin. Sci   Rep 12,   15639   .
401   https://doi.org/10.1038/s41598-022-19775-4 (2022)

402 Boyet, A., De Simone, S., Ge, S. et al. Poroelastic stress relaxation, slip stress transfer and friction
403   weakening controlled post-injection seismicity at the Basel Enhanced Geothermal System.
404   Commun Earth Environ 4, 104. https://doi.org/10.1038/s43247-023-00764-y (2023).

405 Boyet, A., De Simone, S., Vilarrasa, V.; Physics-Based Modeling to Understand and to Propose
406   Forecasting Methods of Induced Seismicity. Seismological Research Letters ; 94 (6): 2666–
407   2678. doi: https://doi.org/10.1785/0220230109, 2023.

408 Carder, D. S. (1945). Seismic investigation in the Boulder Dam area, 1940-1944, and the influence of
409   reservoir loading on earthquake activity, Bull. Seism. Soc. Am. 35, 175-192.(1945).

410 Ceia Marco, Roseane Missagia, Ricardo Fasolo, Irineu Lima Neto, 2019. Relationship between
411   porosity, permeability, and pore compressibility; DOI: 10.22564/16cisbgf 2019.287, 2019

412 CEMIG - Minas Gerais Energy Company (2001). Geological observations in the UHE Irapé sector-
413   Consultancy Report. Belo Horizonte, MG, 6p, 2001

414 Cesca, S., Braun, T., Maccaferri, F., Passarelli, L., Rivalta, E., and Dahm, T. (2013a). Source modelling
415   of the M5–6 Emilia-Romagna, Italy, earthquakes (2012 May 20–29). Geophys. J. Int. 193,
416   1658–1672. doi: 10.1093/gji/ggt069, 2012.

417 Cesca, S., Grigoli, F., Heimann, S., González, Á, Buforn, E., Maghsoudi, S., et al. (2014). The 2013

418 September–October seismic sequence offshore Spain: a case of seismicity triggered by gas

419 injection? Geophys. J. Int. 198, 941–953. doi: 10.1093/gji/ggu172, 2014.

420 Chang, K.W., Yoon, H. Permeability-controlled migration of induced seismicity to deeper depths near

421 Venus in North Texas. Sci Rep 12, 1382 (2022). https://doi.org/10.1038/s41598-022-05242-7,

422 2022.

423 Chen, L., & Talwani, P. (2001). Mechanism of initial seismicity following impound of the

424 Monticello Reservoir, South Carolina. Bulletin of the Seismological Society of America, 91(6),

425 1582-1594, 2001.

426 Chimpliganond, C., G. S. França, A. E. Bandeira, and L. Bevilaqua (2007). Reservoir-triggered

427 seismicity at the highest Brazilian dam, AGU 2007 —Meeting of Americas Joint Assembly

428 Abstract, Acapulco, Mexico, Acapulco, Mexico, 22–25 May, 2007.

429 Cocco, M., Rice, J.M., 2002. Pore pressure and poroelasticity effects in Coulomb stress analysis of

430 earthquake interactions. Journal of Geophysical Research 107. doi:10.1029/2000JB000138,

431 2002.

432 Cornet, F. H., and J. Yin (1995), Analysis of induced seismicity for stress field determination and pore

433 pressure mapping, Pure Appl. Geophysics., 145, 677–700, 1995.

434 CPRM - Mineral Resources Research Company (2004). Project Registration of Groundwater Supply

435 Sources. Jequitinhonha Valley: Diagnosis of the Municipality of Berilo-MG. Belo Horizonte,

436 43p, 2004.

437 Crane, L. J., & Friedman, A. (1956). The diffusion of chemically reacting systems in a laminar flow of

438 fluid. AIChE Journal, 2(2), 186-19, 1956.

439 Developments in Structural Geology and Tectonics, Elsevier, Volume 5, 2019, Pages 119-128,

440 Ellsworth, W. L. (2013). Injection-induced earthquakes. Science 341, 1225942. doi:

441 10.1126/science.1225942, 2013.

442 Foulger, G. R., Wilson, M., Gluyas, J., Julian, B. R., and Davies, R.: Global review of human-induced

443 earthquakes, Earth-Sci. Rev., 178, 438–514, 2018.

444 França, G. S., Assumpção, M., Ribotta, L. C., Von Huelsen, M. G., and Chimpliganond, E. C. N.,

445   Updated compilation of reservoir triggered seismicity in Brazil, in 2010 The Meeting of the

446   Americas (AGU – American Geophysical Union), Foz do Iguaçu, Paraná, Brazil, 2010.

447 Golstein, P; Snoke, A. 2005. "Sac Availability for the Iris Community" Incorporated Institutions for

448   Seismology Data Management Center Eletronic Newsletter. Disponível em: Acessado em: 15

449   de dezembro de 2005.

450 González, P. J., Tiampo, K. F., Palano, M., Cannavó, F., and Fernández, J. (2012). The 2011 Lorca

451   earthquake slip distribution controlled by groundwater crustal unloading. Nat. Geosci. 5, 821–

452   825. doi: 10.1038/ngeo1610, 2012.

453 Gough, D.I., Gough, W.I., 1970a. Stress and deflection in the lithosphere near Lake Kariba, 1. Geophys.

454   J. Int. 21, 65–78, 1970a.

455 Golstein P. & Snoke A. 2005. "Sac Avaliability for the Iris Community" Incorporated Institutions for

456   Seismology   Data   Management   Center   Eletronic   Newsletter.   Disponível   em:

457   www.iris.edu/news/newsletter/vol7no1/page1.htm. Acesso em: 15 dez 2013.

458 Gough, D.I., Gough, W.I., 1970b. Load-induced earthquakes at Kariba, 2. Geophys. J. Int. 21, 79–101,

459   1970b.

460 Grigoli, F., Cesca, S., Rinaldi, A. P., Manconi, A., López-Comino, J. A., Clinton, J. F., et al. (2018). The

461   November 2017 Mw 5.5 Pohang earthquake: a possible case of induced seismicity in South

462   Korea. Science 360, 1003–1006. doi: 10.1126/science.aat 2010, 2018.

463 Gupta, H. K., K. Arora, N. P. Rao, S. Roy, V. M. Tiwari, P. et al., Investigations of continued reservoir

464   triggered seismicity at Koyna, India, Geol. Soc. Lond. Spec. Publ. 445, 151–188 (2016).

465 Gupta, H. K.: A review of recent studies of triggered earthquakes by artificial water reservoirs with

466   special   emphasis   on   earthquakes   in   Koyna,   India,   Earth-Sci.   Rev.   58,   279–310,

467   doi.org/10.1016/S0012-8252(02)00063-6, 2002.

468 Keranen, K. M., Savage, H. M., Abers, G. A., and Cochran, E. S. (2013). Potentially induced

469   earthquakes in Oklahoma, USA: Links between wastewater injection and the 2011 Mw 5.7

470   earthquake sequence. Geology 41, 699–702. doi: 10.1130/ G34045., 2013.

471   Keranen, K. M., Weingarten, M., Abers, G. A., Bekins, B. A., and Ge, S. (2014). Sharp increase in

472   central Oklahoma seismicity since 2008 induced by massive wastewater injection. Science 345,

473   448–451. doi: 10.1126/science.125 5802, 2014.

474   Kim, K.-H., Ree, J.-H., Kim, Y., Kim, S., Kang, S. Y., and Seo, W. (2018). Assessing whether the 2017

475   Mw 5.4 Pohang earthquake in South Korea was an induced event. Science 360, 1007–1009.

476   doi: 10.1126/science. aat6081, 2018.

477   Kivi, I. R., Boyet, A., Wu, H., Walter, L., Hanson-Hedgecock, S., Parisio, F., and Vilarrasa, V.: Global

478   physics-based database of injection-induced seismicity, Earth Syst. Sci. Data, 15, 3163–3182,

479   https://doi.org/10.5194/essd-15-3163-2023, 2023.

480   Lee, W. H. K; Lahr, J. C, 1975. HYPO 1971 (revised a computer program for determining hypocentre,

481   magnitude and first motion pattern of local earthquakes. USGS, Open file report. 64 p., 1975.

482   Lima SAA, Martins-Neto MA, Predrosa-Soares AC, Cordani UG, Nutman A. 2002. The Salinas

483   Formation in the Type Area, NE of Minas Gerais: a proposal to review the stratigraphy of the

484   Araçuaí Belt based on sedimentary and metamorphic evidence and U-Pb SHRIMP ages.

485   Brazilian Journal of Geosciences, 34(4):491-500, 2002.

486   Marshak, S; Alkmim, F. F.; Whittington; Pedrosa-Soares, A. C. 2006. Extensional collapse in the

487   Neoproterozoic Araçuaí orogen, eastern Brazil: a setting for reactivation of asymmetric

488   crenulation cleavage. Journal of Structural Geology, 28(1):129-14, 2006.

489   McGarr, A., Simpson, D., and Seeber, L. (2002). 40—Case histories of induced and triggered seismicity.

490   Int. Geophys. 81A, 647–661, 2002.

491   Neuzil, C. E. (1986). Groundwater flow in low-permeability environments. Water Resources Research,

492   22(8), 1163-1195, 1986.

493   PLANVALE-Water Resources Master Plan for the Jequitinhonha and Pardo Valleys (1994). Diagnostic

494   Report carried out by Geotécnica and DHV Consultants BV, Annex B, Hydrogeology,

495   133p.,1994.

496 Raza, H., Kivi, I.R., França, G.S. and Vilarrasa V. Reservoir impoundment-triggered seismicity in
497   Brazil: the case of M4.0 Nova Ponte earthquake. Sci Rep 13, 22226 (2023).
498   https://doi.org/10.1038/s41598-023-48924-6, 2023.

499 Rice, J.R. and Cleary, M.P. (1976) Some basic stress-diffusion solutions for fluid-saturated elastic
500   porous media with compressible constituents. Rev. Geophys. Space Phys., v.14, pp.227-241,
501   1976.

502 Roeloffs, E.A., 1988. Fault stability changes induced beneath a reservoir with cyclic variations in water
503   level. J. Geophys. Res. 93, 2107–212, 1988.

504 Rutqvist, J. (2012). The geomechanics of CO_2 storage in deep sedimentary formations. Geotechnical
505   and Geological Engineering, 30, 525-551, 2012.

506 Sausse, J., Fourar, M. and Genter, A. (2006) Permeability and alteration within the Soultz granite
507   inferred from geophysical and flow log analysis. Geothermics, v.35(5-6), pp.544-560, 2006.

508 Sayão, E., França, G. S., Holanda, M., and Gonçalves, A.: Spatial database and website for reservoir-
509   triggered seismicity in Brazil, Nat. Hazards Earth Syst. Sci., 20, 2001–2019,
510   https://doi.org/10.5194/nhess-20-2001-2020, 2020.

511 Silva, G. F., J. O. Araújo Filho, M. G. Von Huelsen, C. N. Chimpliganond, and G. S. França (2014).
512   Influence of Brazilian structures on the reservoir-induced seismicity case of Irapé Hydroelectric
513   Plant, Minas Gerais, Brazil, Braz. J. Geol. 44, no. 3, 375–386, DOI: 10.5327/Z2317-
514   4889201400030004, 2014.

515 Simpson, D.W. (1976) Seismicity change associated with the reservoir loading. Engg. Geol., v.10,
516   pp.123-150, 1976

517 Simpson, D.W., Leith, W.S. and Scholz, C.H. (1988) Two types of reservoirs induced seismicity. Bull.
518   Seism. Soc. Amer., v.78, pp.2025–2040, 1988.

519 Simpson, DW 1986. Triggered Earthquakes. Annual Review Earth Planetary Sciences, 14: 21-42, 1986.

520 Skempton, A. W. (1954). The pore-pressure coefficients A and B. Geotechnique, 4(4), 143-14, 1954.

521   Snow, D.T., 1972. Geodynamics of seismic reservoirs. Proceedings of the Symposium on Percolation

522   through Fissured Rocks. Deutsche Gessellschaft für Erd- und Grundbau, Stuttgart, Germany,

523   pp. 1–19 (T2-J), 1972.

524   Talwani, P. and Acree, S. (1984/85), Pore pressure diffusion and mechanism of reservoir induced

525   seismicity. Pure and applied Geophysics 122,947-965, 1984/85.

526   Todd, D. K., & Mays, L. W. (2005). Groundwater Hydrology, 2005.

527   Vilarrasa, V., Carrera, J., Olivella, S., Rutqvist, J., and Laloui, L.: Induced seismicity in geologic carbon

528   storage, Solid Earth, 10, 871–892, https://doi.org/10.5194/se-10-871-2019, 2019.

529   Vilarrasa, V., De Simone, S., Carrera, J. et al. Multiple induced seismicity mechanisms at Castor

530   underground gas storage illustrate the need for thorough monitoring. Nat. Commun. 13, 3447

531   (2022). https://doi.org/10.1038/s41467-022-30903-6, 2022.

532   Vilarrasa, V., De Simone, S., Carrera, J., and Villaseñor, A.: Unravelling the causes of the seismicity

533   induced by underground gas storage at Castor, Spain, Geophys. Res. Lett., 48, e2020GL092038,

534   https://doi.org/10.1029/2020GL092038, 2021.

535   Vilarrasa, V., Makhnenko, R. & Gheibi, S. 2016. Geomechanical analysis of the influence of CO_2

536   injection location on fault stability. Journal of Rock Mechanics and Geotechnical Engineering.

537   8(6):805–818, 2016.

538   Vilarrasa, V., Raza, H., Kivi, I. R., and França, G. S.: Understanding the triggering mechanisms of

539   reservoir-triggered seismicity at Nova Ponte, Brazil, through hydro-mechanical modeling, EGU

540   General Assembly 2023, Vienna, Austria, 24–28 Apr 2023, EGU23-11711,

541   https://doi.org/10.5194/egusphere-egu23-11711, 2023.

542   Wever, T. H. 1989. The Conrad discontinuity and the lop of the reflective lower crust – do they coincide?

543   Tectonophysics,157:39-58, 1989.

544   Yeck, W. L., Weingarten, M., Benz, H. M., McNamara, D. E., Bergman, E. A., Herrmann, R. B., et al.

545   (2016). Far-field pressurization likely caused one of the largest injections induced earthquakes

546   by reactivating a large preexisting basement fault structure. Geophys. Res. Lett. 43, 10198–

547   10207. doi: 10.1002/2016GL07 0861, 2016.

548